Engineering Transactions, **74**(1): 105–120, 2026, https://doi.org/10.24423/engtrans.2025.3484
Institute of Fundamental Technological Research Polish Academy of Sciences (IPPT PAN)
Université de Lorraine • Poznan University of Technology

SiMRTRANS

Simulation of Vibro-Isolation Performance in Sensitive Cargo Transportation Platforms with Quasi-Zero-Stiffness Suspension under Impact Perturbations

Oleksiy Larin[1)*], Ksenia Potopalska[1)], Galina Timchenko[2)], Nikita Vasylchenko[1)]

[1)] *Department of Mathematical Modeling and Intelligent Computing in Engineering*
[2)] *Department of Applied Mathematics*
National Technical University "Kharkiv Polytechnic Institute"
Kharkiv, Ukraine

[*]Corresponding Author: oleksiy.larin@khpi.edu.ua

This work deals with the theoretical modeling of the vertical dynamics of a specialized vehicle featuring a dual suspension system. Vehicle ride quality is essential for ensuring the safety and comfort of passengers and the protection of sensitive or hazardous cargo. The study focuses on a two-axle vehicle model with a dual suspension system. The first-level comprises a traditional suspension with linear stiffness, while the second-level features nonlinear quasi-zero-stiffness (QZS) characteristics. The research employs a discrete nonlinear dynamic model that considers the vertical displacements and angular rotations of the vehicle masses. The nonlinear QZS response is modeled to optimize vibration isolation performance under varying load conditions, while damping effects are included via a Rayleigh dissipation function. The integral characteristics of the QZS element are also studied in detail using finite element (FE) computer simulations in a 3D setting. These simulations provide a comprehensive understanding of the mechanical response and stress-strain distribution within the QZS element, validating its performance under real-world conditions. The results demonstrate the influence of the nonlinear suspension characteristics on vibration isolation performance and load stability. The QZS-based suspension effectively reduces dynamic stresses, particularly under low-frequency excitations, while maintaining structural integrity and operational efficiency.

Keywords: vibro-isolation performance, nonlinear discrete model, kinematic excitations, quasi-zero stiffness, meta-structures.

1. Introduction

Vehicle ride quality constitutes a critical parameter for the secure and comfortable transportation of passengers and goods within automotive systems.

For specific cargo types – such as vibration-sensitive or hazardous materials – it is essential to attenuate dynamic loads to mitigate the risk of damage or safety incidents. These dynamic stresses, which impact cargo, are primarily induced by road surface irregularities that propagate forces through the vehicle's wheels and suspension architecture. Nonlinear suspension solutions, especially those designed with variable stiffness and damping properties [1, 2], are therefore essential in modern automotive engineering, providing an optimal balance between vibration isolation and operational efficiency under varying conditions. By reducing dynamic loads, these systems not only improve stability and comfort for passengers, but also protect sensitive or dangerous loads from potential damage. This approach is particularly important on uneven road surfaces, where the forces transmitted through the suspension could otherwise create excessive stress on both passengers and cargo.

In contemporary engineering practice, nonlinear suspension systems with adaptive stiffness or damping characteristics are extensively employed to suppress dynamic loads during transit. Among these, suspensions exhibiting quasi-zero stiffness (QZS) properties are particularly significant, as they provide effective vibration isolation while maintaining suspension effectiveness. Such systems perform optimally under certain operational conditions and are advantageous due to their compact configurations, which facilitate efficient spatial integration [3–6].

From an engineering point of view, QZS elements can be realized using different technical schemes. For example, a gas-interconnected QZS pneumatic suspension was presented in [7, 8], where an X-shaped structure was designed. Studies [9–11] examined various models of vibration isolators aimed at enhancing vibration isolation efficiency.

It was proposed in [12] to use an isolator consisting of n consecutive elements to study the mechanism of acquiring multiple QZS characteristics. Three types of equivalent mechanical models were studied to investigate the properties of the proposed isolator. It was found that, as the number of layers increased, the proposed isolator was effective in achieving low-frequency vibration isolation under different preloads, and this advantage could be further enhanced with small damping and excitation. A single-degree-of-freedom (DOF) system incorporating the proposed isolator was developed for theoretical and experimental study of its isolation characteristics in [12, 13]. A numerical method, based on the direct integration of the dynamic equation, verified the analytical results of the frequency response functions. Experiments were also carried out to verify the isolation performance of the nonlinear vibrator supported by the flexible plate.

Generally, it can be concluded that negative stiffness, which arises in unit cells through buckling or snap-through, is considered the fundamental principle

for energy absorption [5, 10–12, 14]. That is, by appropriately assembling unit cells with negative stiffness in series, metamaterials and/or metastructures can be developed with desired shock protection or energy absorption performance [10, 12]. Specially designed curved beams and inclined beams [5, 10–12, 14], placed within constrained supporting frames, can be easily fabricated using 3D printing technology.

Based on the different approaches described, one can find that recent advances in metastructures and additive technologies provide new technologically efficient and cost-effective tools to realize QZS elements and integrate them into the suspension system of modern specialized vehicles.

The current study considers the theoretical modeling of the dynamic behavior of a specialized vehicle with a dual suspension system. The first-level is a typical torsion bar suspension with linear stiffness, while the second-level has a nonlinear characteristic with QZS and serves as a third vibration isolation/damping element, in particular one with an internal elastic-damper support. The modeling is presented within the framework of numerical vibration analysis, based on a discrete nonlinear dynamic system. The dynamics of the system are analyzed under a kinematic impact load sequentially applied to the front and rear axles of the vehicle.

2. Discrete model of the specialized vehicle with nonlinear double-level suspension

A two-axle vehicle is considered, the model of which is shown in Fig. 1. It conditionally consists of three levels: the basic suspension, the platform, and the vibration isolation object. The vehicle base has a linear suspension, while the cargo platform is equipped with an additional suspension stage. This stage is connected to the first-level suspension through an additional second-level that exhibits a nonlinear elastic response with QZS (Fig. 1).

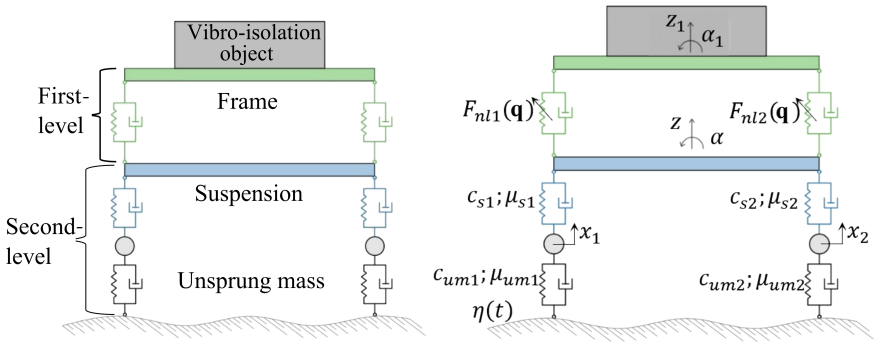

Fig. 1. General schematic of the proposed dynamic system with a double-level suspension.

Lagrange's second-order equations are used to develop a discrete nonlinear model according to the proposed vehicle design, technical scheme of which is shown in Fig. 1:

$$\frac{\mathrm{d}}{\mathrm{d}t}\left(\frac{\partial T}{\partial \dot{q}_i}\right)+\frac{\partial T}{\partial \dot{q}_i}+\frac{\partial \Pi}{\partial q_i}+\frac{\partial R}{\partial \dot{q}_i}=0, \qquad i=\overline{1,...,6}, \tag{2.1}$$

where t denotes time, T is the kinetic energy of the system, Π is the potential energy of the system, and R is the potential of the dissipative forces, q_i is the generalized coordinate, which consist of the vertical motions of the masses and the angles of the rotations (Eq. (2.2)). The dots above the variables indicate time derivatives:

$$\{\mathbf{q}\}=\{x_1,x_2,z,\alpha,z_1,\alpha_1\}^{\mathrm{T}}. \tag{2.2}$$

It is straightforward to obtain the kinetic energy:

$$T=\frac{1}{2}\sum_{i=1}^{6}m_i\dot{q}_i^2, \tag{2.3}$$

where m_1 is the total front axle mass, which consists of two wheels and the axle shaft, the same applies to the rare axle mass $m_2=m_1$. The mass m_3 designates the total suspension mass (with all installed units) of the first-level. The mass $m_4=m_{fr}+m_o$ is the total mass of the second-level of suspension, which includes the cargo frame (m_{fr}) and the mass of the vibration isolation object (m_o). The moments of inertia of the first-level frame as well as the second-level frame (generally a specific cargo platform) are denoted as $m_5=J_1$ and $m_6=J_2$, respectively.

The system potential energy consists of the potential energy of the linear elastic elements (the tires and the first-level suspension) and the potential energy of the nonlinear suspension system of the second-level:

$$\Pi=\Pi_l+\Pi_{nl}. \tag{2.4}$$

The linear part can be presented as follows:

$$\Pi_l=\frac{1}{2}\sum_{i=1}^{2}c_{umi}\left(x_i-\eta_i(t)\right)^2+\frac{1}{2}\sum_{i=1}^{2}c_{si}\left(z-x_{1i}\right)^2, \tag{2.5}$$

where the following designations are additionally used:

$$x_{11}=z-\frac{L}{2}\alpha, \qquad x_{12}=z+\frac{L}{2}\alpha. \tag{2.6}$$

The potential energy of the second-level suspension is defined as the integral of the nonlinear elastic response, i.e., $F_{nl}(y) = (\partial \Pi_{nl})/(\partial y)$. Considering that there are two nonlinear elements presented in the system (front and rear), the following equation for Π_{nl} can be written using the notations shown in Fig. 1:

$$\Pi_{nl}(z, z_1, \alpha, \alpha_1) = \Pi_{nl1}(y_1 = z_1 - x_{21}) + \Pi_{nl2}(y_2 = z_1 - x_{22}), \tag{2.7}$$

where

$$x_{21} = z_1 - z + \frac{L}{2}(\alpha - \alpha_1), \qquad x_{22} = z_1 - z + \frac{L}{2}(\alpha_1 - \alpha). \tag{2.8}$$

Considering the correspondence between local and global coordinates, the following formulations for the nonlinear forces can be proposed:

$$F_3 = \frac{\partial \Pi_{\mathrm{nl1}}}{\partial y_1}\frac{\partial y_1}{\partial z} + \frac{\partial \Pi_{\mathrm{nl2}}}{\partial y_2}\frac{\partial y_2}{\partial z} = -\left[F_{nl}(y = z_1) + F_{nl}(y = z_2)\right], \tag{2.9}$$

$$\widetilde{F}_3 = \frac{\partial \Pi_{nl1}}{\partial y_1}\frac{\partial y_1}{\partial \alpha} + \frac{\partial \Pi_{nl2}}{\partial y_2}\frac{\partial y_2}{\partial \alpha} = \frac{L}{2}\left[F_{nl}(y = z_1) - F_{nl}(y = z_2)\right], \tag{2.10}$$

$$F_4 = \frac{\partial \Pi_{\mathrm{nl1}}}{\partial y_1}\frac{\partial y_1}{\partial z_1} + \frac{\partial \Pi_{\mathrm{nl2}}}{\partial y_2}\frac{\partial y_2}{\partial z_1} = F_{nl}(y = z_1) + F_{nl}(y = z_2), \tag{2.11}$$

$$\widetilde{F}_4 = \frac{\partial \Pi_{nl1}}{\partial y_1}\frac{\partial y_1}{\partial \alpha_1} + \frac{\partial \Pi_{nl2}}{\partial y_2}\frac{\partial y_2}{\partial \alpha_1} = \frac{L}{2}\left[-F_{nl}(y = z_1) + F_{nl}(y = z_2)\right]. \tag{2.12}$$

The dissipative forces in the current study are proposed to be considered within a Rayleigh linear model, in which the damping matrix is proportional to the linear stiffness matrix. Therefore, the damping potential is a quadratic form of the generalized coordinate velocities.

Substituting Eq. (2.3) and Eq. (2.4), and considering Eq. (2.5) to Eq. (2.12), into the Lagrange Eq. (2.13), one can obtain the main system of equations:

$$\begin{cases} m_1\ddot{x}_1 + \dfrac{\partial R}{\partial \dot{x}_1} + F_{el1} = c_t\eta_1(t), \\ m_2\ddot{x}_2 + \dfrac{\partial R}{\partial \dot{x}_2} + F_{el2} = c_t\eta_2(t), \\ m_3\ddot{z} + \dfrac{\partial R}{\partial \dot{z}} + F_{el3} + F_3(z, z_1, \alpha, \alpha_1) = 0, \\ J_1\ddot{\alpha} + \dfrac{\partial R}{\partial \dot{\alpha}} + F_{el4} + \widetilde{F}_3(z, z_1, \alpha, \alpha_1) = 0, \\ m_4\ddot{z}_1 + \dfrac{\partial R}{\partial \dot{z}_1} + F_4(z, z_1, \alpha, \alpha_1) = 0, \\ J_2\ddot{\alpha}_1 + \dfrac{\partial R}{\partial \dot{\alpha}_1} + \widetilde{F}_4(z, z_1, \alpha, \alpha_1) = 0. \end{cases} \tag{2.13}$$

Thus, we have a system of differential equations describing the dynamics of a vehicle with a double-level nonlinear suspension, where the second-level is additional and exhibits nonlinear characteristic. In system (2.13), to simplify the presented form of the equations, a vector of elastic forces ($\mathbf{F}_{el}$) is introduced:

$$\{\mathbf{F}_{el}\} = [\mathbf{K}]\,\{\mathbf{q}\}\,, \tag{2.14}$$

$$[\mathbf{K}] = \begin{bmatrix} (c_{um1}+c_{s1}) & 0 & -c_{s1} & \frac{L}{2}c_{s1} & 0 & 0 \\ & (c_{um2}+c_{s2}) & -c_{s2} & -\frac{L}{2}c_{sa} & 0 & 0 \\ & & c_{ss} & -\frac{L}{2}c_{sn} & 0 & 0 \\ & & & L^2\frac{c_{ss}}{4} & 0 & 0 \\ & \text{symmetric part} & & & 4c_{fr} & 0 \\ & & & & & L^2c_{fr} \end{bmatrix}, \tag{2.15}$$

where, for simplification, we introduced additional parameters for the total stiffness of the first-level of suspension and for the difference between the front and rear axle stiffness of the first-level suspension:

$$c_{ss} = c_{sn1} + c_{sn2}, \qquad c_{sn} = c_{sn2} - c_{sn1}. \tag{2.16}$$

In the stiffness matrix, an additional parameter c_{fr} is introduced. It is artificially added as a linearized (through bisection approximation) stiffness of the second-level suspension. The derived elastic forces $\mathbf{F}_{el5}$ and $\mathbf{F}_{el6}$ are not used directly in Eq. (2.13); however, the stiffness matrix in its full size is used for the introduction of damping and for some calculations of natural frequencies and normal modes, which are used for model testing and basic preliminary dynamic analysis.

Additionally, the system of (2.13) includes some dissipative forces, which reflect the presence of viscosity in tire deformation and damping in the first-level suspension. These forces are derived from the corresponding potential of dissipative forces (2.9) and have the following analytical expressions, given in matrix form as follows:

$$\left\{\frac{\partial R}{\partial \dot{q}}\right\} = \mu\,[\mathbf{K}]\,\{\dot{q}\}. \tag{2.17}$$

The system (2.13) allows the analysis of vertical and angular vibrations of the vehicle occurring under the kinematic excitations $\eta_1(t)$ and $\eta_2(t)$, which are

applied to the wheels of the vehicle due to interaction with road surface roughness. Here, it must be underlined that a time delay must be taken into account and then the kinematic load is applied:

$$\eta_1(t) = \eta(t), \qquad \eta_2(t) = \eta\left(t + \frac{L}{v}\right), \tag{2.18}$$

where L is the distance between the wheel axles and v is the vehicle riding speed.

A simple perturbation is introducing here as a half-sinusoidal function of time:

$$\eta(t) = \begin{cases} a_0 \sin \dfrac{\pi\,(t - t_0)}{t_n - t_0}, & t \in [t_0, t_n]\,, \\ 0, & t \notin [t_0, t_n], \end{cases} \tag{2.19}$$

where a_0 is the amplitude (height) of the geometric perturbation, and t_0, t_n are, respectively, the initial and final times during which the perturbation is active. The value of t_n is calculated from the geometric size (width) of the perturbation and the vehicle riding speed.

Presented system of (2.13) is identified with the nonlinear elastic forces $F_{nl}(y)$. In the current work, we propose to use a specific element that has a QZS of its elastic response. In this study, we numerically identified such a response of the QZS element and approximated the resulting dependencies using cubic splines. Some details for this element modeling are presented further.

3. Integral nonlinear elastic response of the QZS element

Following the idea of repetitive elementary cells in metamaterials proposed in [10], in the current study, we use QZS elements, which are formed by a sinusoidal beam, a pair of semicircular arches, and stiffer wall elements.

The 3D model was build in parametric form, allowing us to determine rational geometrical parameters of the QZS element that has a QZS response region within a required range of possible displacements. Our model also ensures a practically required level of response forces, which enable the use of such an element in real applications. Finite element (FE) modeling is used for direct computer simulations, which allow us to obtain the integral elastic response of the QZS element under kinematic (displacement-controlled) loading. Figure 2 presents the geometry and FE mesh.

The final model parameters allow us to obtain the nonlinear characteristic of the QZS element, which yields an almost zero reaction to displacement perturbations in a region of 30 mm. The corresponding results of computer simulations are presented in Fig. 3.

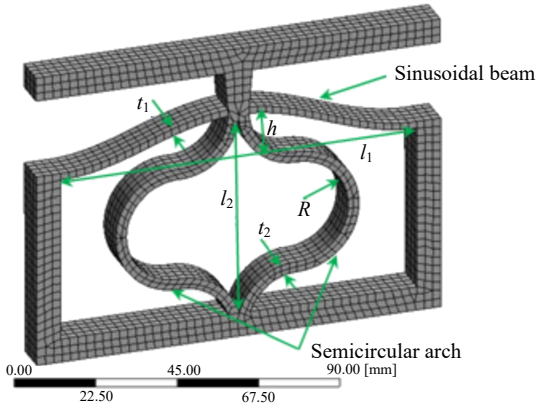

Fig. 2. QZS element FE model and geometry.

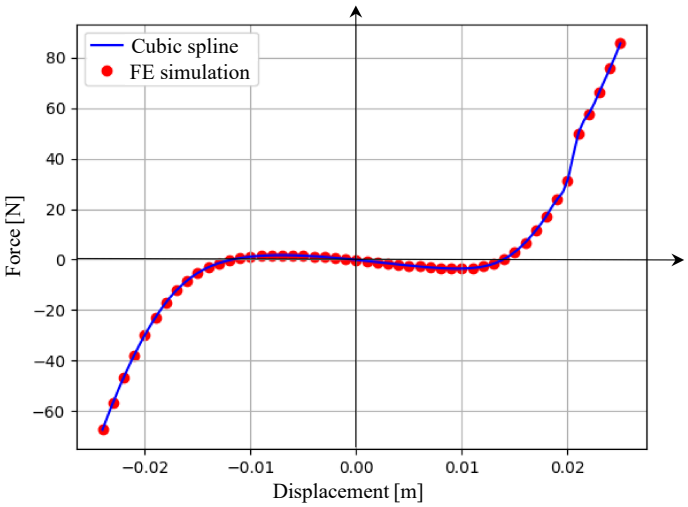

Fig. 3. Integral nonlinear elastic response of QZS element.

The main geometric parameters of the QZS element, determined from a set of FE simulations and used as the basic model in the current study, are as follows: $l_1 = 208\,\text{mm}$ (width), $l_2 = 120\,\text{mm}$ (hight), $l_3 = 14\,\text{mm}$ (thickness), $t_1 = 8.1\,\text{mm}$ (beam thickness), $t_2 = 12.4\,\text{mm}$ (arc thickness), $h = 31.5\,\text{mm}$, and $R = 30\,\text{mm}$.

It should be noted that if the potential displacements exceed the specified values, the stiffness of this system will lead to the opposite effect in terms of vibration isolation. This unit element demonstrates satisfactory results and can serve as a basis for modeling a more complex vibration isolator that can operate at higher displacement levels. Figure 3 shows these results, which are centered around zero when considering the mean static load.

FE simulations also allow us to determine and evaluate additional strength parameters of the QZS element. This is important from a practical perspective to

ensure reliability. Figure 4 demonstrates the distributions of displacements (deformation filed) and von Mises stresses at different levels of displacement-controlled loading with an amplitude of ±9 mm.

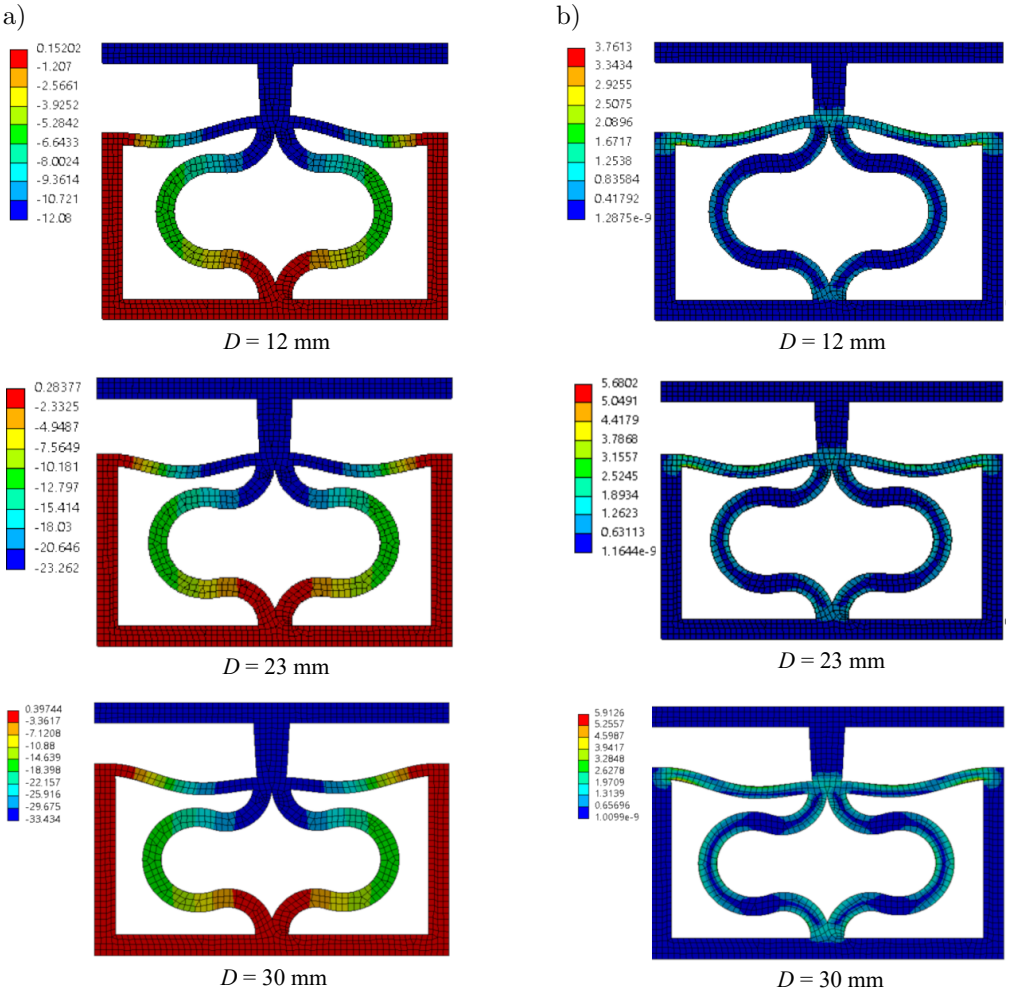

Fig. 4. a) Vertical displacements [mm], b) equivalent von Mises stresses [MPa] under different displacement-controlled load levels load.

4. Results of the numerical simulations of vibro-isolation performance for sensitive cargo transportation

Mathematical model presented in Sec. 2, with nonlinear elastic responses F_{nl} of QZS elements identified from direct FE simulations, is used for numerical computations of the dynamics of such a system. The differential Eq. (2.13) are solved numerically using an explicit integration scheme. The mechanical and

geometrical parameters used in the numerical experiments are summarized in Table 1.

Table 1. Mechanical parameters of the system.

Parameter	L	m_1, m_2	m_3	m_4	I_1	I_2	c_{sn1}, c_{sn2}	c_{um}
Units	m	kg	kg	kg	kg m^2	kg m^2	kN/m	kN/m
Value	2.2	83	168	176	252.3	344.6	240	350

As a results of the integration, we obtained the dynamics of all generalized coordinates, including displacements, velocities, and accelerations. Figure 5 and Fig. 6 present examples of the computed time histories for vertical vibrations of the front and rear axes, as well as vertical vibrations of the center of mass at

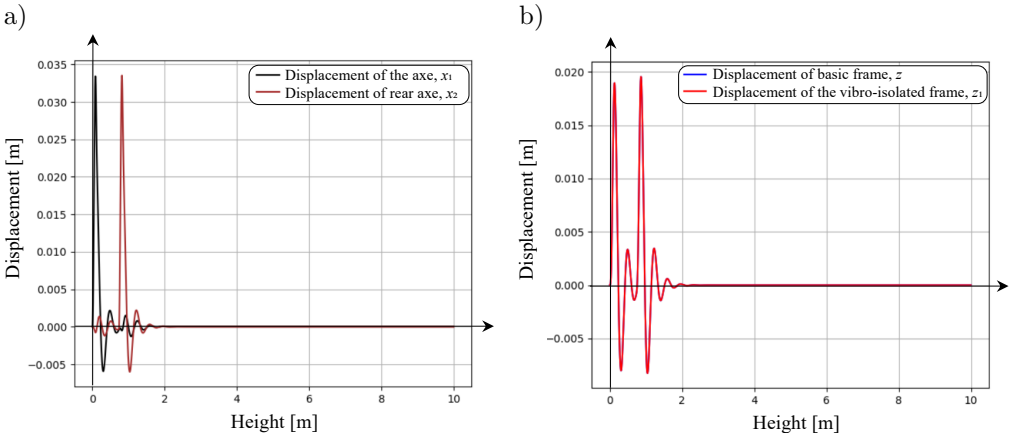

Fig. 5. Vertical vibrations of the generalized coordinates of the vehicle without the second-level of nonlinear suspension (model L).

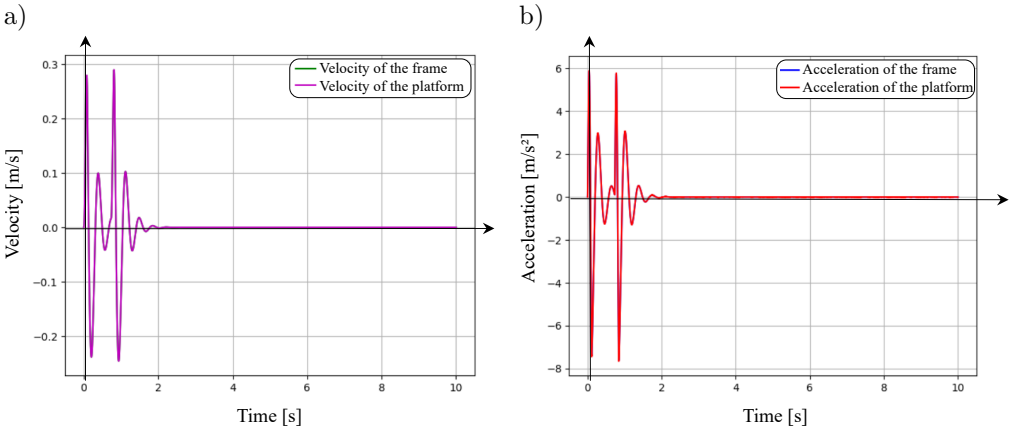

Fig. 6. Vertical velocity and acceleration of the cargo object's center of mass.

the first- and second-level suspension, i.e., z and z_1. In this example, the road roughness has a height of 50 mm and a width of 300 mm (standard road).

These results are presented for the case where second-level suspension is excluded from the model. Technically, this is realized by substituting the nonlinear forces with linear ones of extremely high stiffness (10^8 N/m), which corresponds to a rigid metal rod connection between the suspension levels. This approach allows us to maintain the same mass-inertial properties in both models: the basic linear model (model L) and the double-level nonlinear model (model NL).

Figure 6 shows the time dependencies of vibro-velocities and vibro-accelerations in the centre of mass of the cargo object (the object subject to potential vibro-isolations) for model L.

The same results were obtained for the proposed system with a second-level suspension integrating nonlinear QZS elements (model NL). Figure 7 and Fig. 8

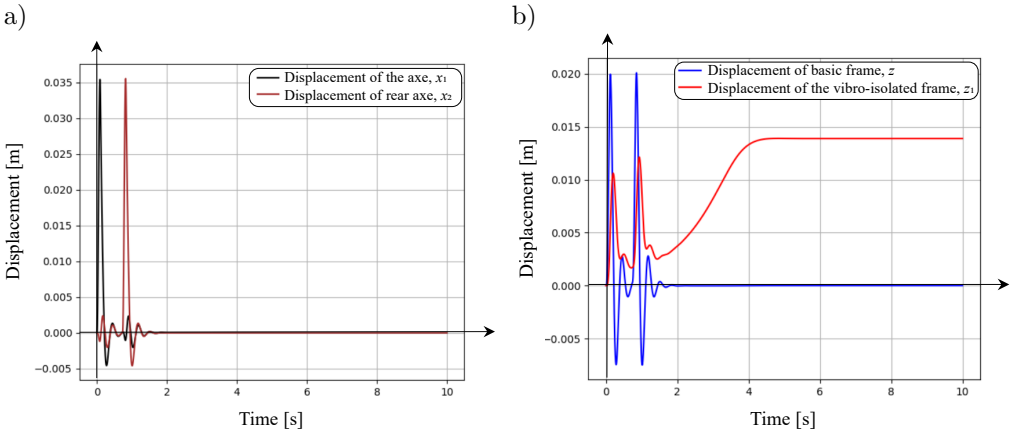

Fig. 7. Vertical vibrations of the generalized coordinates of the vehicle with the second-level of nonlinear suspension (model NL).

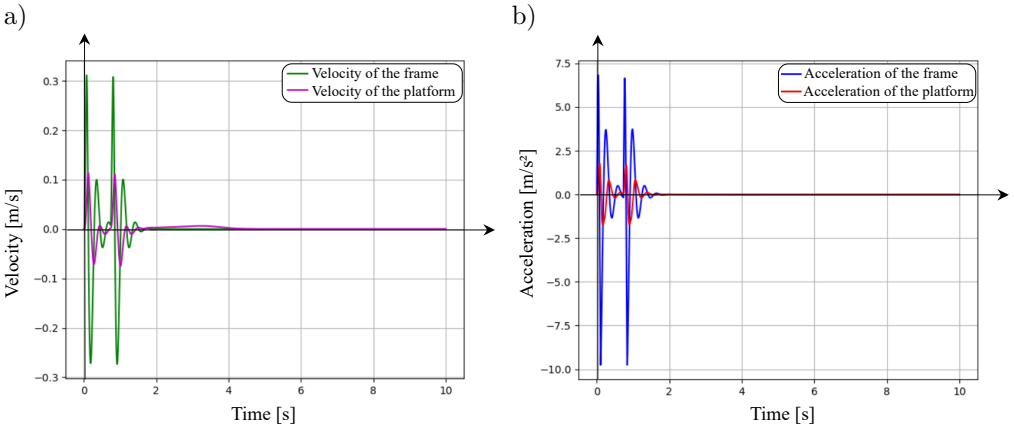

Fig. 8. Vertical vibrations of the generalized coordinates of the vehicle with the second-level of nonlinear suspension (model NL).

show the results for this case. Vertical vibrations of the front and rear axes have similar behavior and amplitudes levels as well as vertical dynamics of the center of mass as in the first-level suspension. However, the center of mass of the second-level simulation, which actually corresponds to the cargo object (the object being vibro-isolated) shows a significant reduction in vibration amplitudes at the moments of impact. An interesting phenomena is also observed: the displacement (position) of the cargo object's center of mass exhibits a smooth shifting over time following the impacts. This post-impact behavior is likely caused by inertia effects and shows a negative phenomena of some energy accumulation in the QZS elements.

Analysis of the vibro-velocity and vibro-acceleration levels shows a triple reduction in the amplitude levels, which confirms the crucial effectiveness of integrating QZS elements into the second-level suspension.

In the current study, a series of comparative computations was carried out to analyze vertical vibrations (displacements, velocities, and accelerations) under varying levels and shapes of kinematic impacts. We have varied the amplitude of the impact (height of the road roughness) in the range from 10 mm to 100 mm but with a fixed time of the impact (corresponding to a road roughness width of 300 mm). The results of these calculations are shown in Fig. 9. The proposed system of vibro-isolations shows a good efficiency in reducing vertical vibrations for impacts with amplitudes up to 70 mm, achieving a maximum reduction of nearly 100 %. In Fig. 9, phase trajectories of the vertical vibrations are also plotted for additional insight.

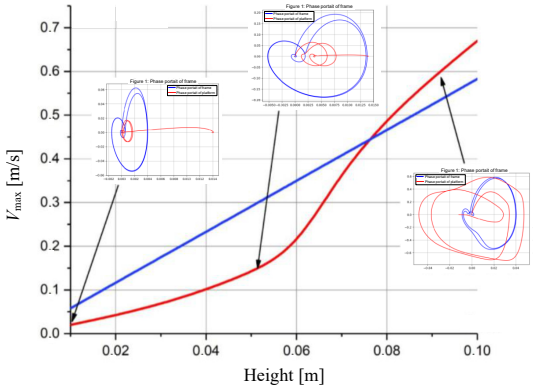

Fig. 9. Vertical vibrations of the center of mass of the vibro-isolated object (model L – blue line, model NL – red line).

Additionally, we examined the influence of the impact width on vibro-isolation performance. The results presented in Fig. 10 and Fig. 11 show that, as the road roughness width increases, the amplitudes of vibro-velocities and vibro-

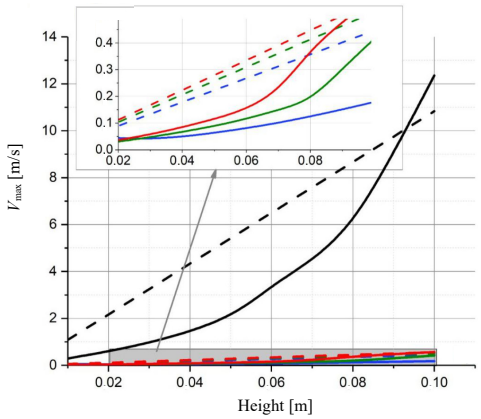

FIG. 10. Vertical vibro-velocities of the center of mass of the vibro-isolated object as a function of kinematic impact width (model L – dashed line, model NL – solid line).

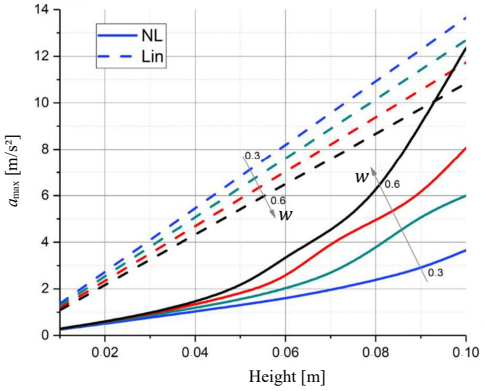

FIG. 11. Vertical accelerations of the center of mass of the vibro-isolated object as a function of kinematic impact width (model L – dashed line, model NL – solid line).

accelerations rise in the nonlinear model, whereas they increase only slightly and almost linearly in the linear model. Despite this, the nonlinear model consistently demonstrates good efficiency up to 90 mm for the road roughness height. For instance, at a 60 mm impact height and a 0.6 m width, we observed a two-fold reduction in vibro-accelerations.

5. Conclusion

The presented study highlights advancements in suspension systems for specialized vehicles, emphasizing the integration of nonlinear and QZS elements to enhance ride quality and vibration isolation. By combining linear and nonlinear suspension levels, the proposed dual-suspension system effectively minimized dynamic loads, protecting both passengers and cargo. Leveraging modern meta-

structural designs and additive manufacturing, the system achieved compact and cost-efficient configurations suitable for various operational conditions.

Numerical simulations demonstrated the significant effectiveness of the QZS-integrated suspension system. We observed a threefold reduction in vibro-velocity and vibro-acceleration amplitudes when comparing the QZS model to the basic linear model. The system effectively reduced vertical vibration amplitudes for kinematic impacts up to 70 mm in height.

An intriguing phenomenon was also observed: after impacts, the displacement (position) of the cargo object's center of mass exhibited a smooth, prolonged shift over time. This post-impact behavior, likely due to inertial effects, suggests negative phenomenon of a potential energy accumulation in the QZS elements. For improved system behavior in operational scenarios, an automatic positioning system and specific control strategy may need to be developed.

Fundings

This scientific study was supported and partially funded by National Research Foundation of Ukraine (NRFU grant no. 2023.03/0255).

Conflict of interest

The authors declare that they have no known competing financial interests or personal relationships that could have appeared to influence the work reported in this paper.

Authors' contributions

Oleksiy Larin formulated the general research problem, coordinated the overall study design, developed the Python-based computational tools used for post-processing and analysis, and interpreted the obtained results. He also prepared the final conclusions of the study. Galina Timchenko developed the mathematical model of the vehicle system, derived the governing differential equations, and performed the numerical simulations of the dynamic response. She also contributed to data processing, visualization of simulation results, and their analytical interpretation. Ksenia Potopalska designed the quasi-zero-stiffness (QZS) meta-structure concept and carried out the analysis of the integral nonlinear elastic characteristics of the QZS element. She was responsible for incorporating these characteristics into the mathematical model of the vibro-isolation system. Nikita Vasylchenko developed and verified the three-dimensional finite element model of the QZS meta-structure and conducted the finite element simulations used to evaluate deformation behavior, stress–strain states, and mechanical response of the QZS element. All authors reviewed and approved the final manuscript.

Data availability statement

Some or all of the data, models, or code that support the findings of this study are available from the corresponding author upon request.

References

1. Jin Y., Hou S., Yang T., Cascaded essential nonlinearities for enhanced vibration suppression and energy harvesting, *Nonlinear Dynamics*, **103**(2): 1427–1438, 2021, https://doi.org/10.1007/s11071-020-06165-6.
2. Fidrovska N., Slepuzhnikov E., Larin O., Varchenko I., Lipovyi V., Afanasenko K., Harbuz S., Increase of operating reliability of the travel wheel using the use of the elastic inserts EUREKA, *Physics and Engineering*, **2020**(5): 69–79, 2020, https://doi.org/10.21303/2461-4262.2020.001387.
3. Wang K., Zhou J., Chang Y., Ouyang H., Xu D., Yang Y., A nonlinear ultra-low-frequency vibration isolator with dual quasi-zero-stiffness mechanism, *Nonlinear Dynamics*, **101**(2): 755–773, 2020, https://doi.org/10.1007/s11071-020-05806-0.
4. Yan B., Yu N., Ma H., Wu C., A theory for bistable vibration isolators, *Mechanical Systems and Signal Processing*, **167**(Part A): 108507, 2022, https://doi.org/10.1016/j.ymssp.2021.108507.
5. Yan B., Wang Z., Ma H., Bao H., Wang K., Wu C., A novel lever-type vibration isolator with eddy current damping, *Journal of Sound and Vibration*, **494**: 115862, 2021, https://doi.org/10.1016/j.jsv.2020.115862.
6. Bian J., Jing X., Analysis and design of a novel and compact X-structured vibration isolation mount (X-mount) with wider quasi-zero-stiffness range, *Nonlinear Dynamics*, **101**(4): 2195–2222, 2020, https://doi.org/10.1007/s11071-020-05878-y.
7. Jiang X., Xu X., Shi T., Atindana V.A., Nonlinear characteristic analysis of gas-interconnected quasi-zero stiffness pneumatic suspension system: A theoretical and experimental study, *Chinese Journal of Mechanical Engineering*, **37**(1): 58, 2024, https://doi.org/10.1186/s10033-024-01039-z.
8. Pu H., Yuan S., Peng Y., Meng K., Zhao J., Xie R., Huang Y., Sun Y., Yang Y., Xie S., Luo J., Chen X., Multi-layer electromagnetic spring with tunable negative stiffness for semi-active vibration isolation, *Mechanical Systems and Signal Processing*, **121**: 942–960, 2019, https://doi.org/10.1016/j.ymssp.2018.12.028.
9. Lu Z.-Q., Gu D.-H., Ding H., Lacarbonara W., Chen L.-Q., Nonlinear vibration isolation via a circular ring, *Mechanical Systems and Signal Processing*, **136**: 106490, 2020, https://doi.org/10.1016/j.ymssp.2019.106490.
10. Fan H., Yang L., Tian Y., Wang Z., Design of metastructures with quasi-zero dynamic stiffness for vibration isolation, *Composite Structures*, **243**: 112244, 2020, https://doi.org/10.1016/j.compstruct.2020.112244.
11. Gholikord M., Etemadi E., Imani M., Hosseinabadi M., Hu H., Design and analysis of novel negative stiffness structures with significant energy absorption, *Thin-Walled Structures*, **181**: 110137, 2022, https://doi.org/10.1016/j.tws.2022.110137.
12. Dalela S., Balaji P.S., Leblouba M., Trivedi S., Kalam A., Nonlinear static and dynamic response of a metastructure exhibiting quasi-zero-stiffness characteristics for

vibration control: An experimental validation, *Scientific Reports*, **14**(1): 19195, 2024, https://doi.org/10.1038/s41598-024-70126-x.

13. Hao R.-B., Lu Z.-Q., Ding H., Chen L.-Q., A nonlinear vibration isolator supported on a flexible plate: analysis and experiment, *Nonlinear Dynamics*, **108**(2): 941–958, 2022, https://link.springer.com/article/10.1007/s11071-022-07243-7.
14. Debeau D.A., Seepersad C.C., Haberman M.R., Impact behavior of negative stiffness honeycomb materials, *Journal of Materials Research*, **33**: 290–299, 2018, https://doi.org/10.1557/jmr.2018.7.

Received December 13, 2024; revised June 1, 2025; accepted July 14, 2025; available online December 16, 2025; version of record March 13, 2026; published issue March 30, 2026.